Indian J. Phys. **52B**, 237–256 (1978)

Current trends in atomic collision experiments

S. B. KARMOHAPATRO

Saha Institute of Nuclear Physics, Calcutta 700009

1. INTRODUCTION

Experimental studies on atomic collision processes are as old as the discovery of the electrical discharges in gases. However, in the first stage of the systematic study, experimental data on outershell excitation and ionisation were accumulated with the projectile ion beam not usually mass analysed. In a later period of this stage mass analysed ion beam was used. The use of an electromagnetic isotope separator as a low energy accelerator producing 10–100 keV mass analysed ion beam was initiated by Kistemaker and his group for outer shell ionisation and excitation experiments (Karmohapatro 1976, Van Eck *et al* 1962, Van Eck and Kistemaker 1960, Sluyters 1959, de Heer 1956).

In recent years, more sophisticated experimental methods (Massey and Gilbody, 1974) like velocity selection using rotating slotted discs, merging beam and crossed beam techniques have been introduced for increasing sensitivity of detection, eliminating background effects, attaining high angular resolution and for obtaining results for ions of energy as low as in the electron volt region. The experiments have been extended to heavy ion induced inner shell ionisation with X-ray emission and to study the channeling phenomena due to impact of heavy ions in solids. Beam foil spectroscopy, ion scattering spectrometry and secondary ion mass spectrometry are modern techniques for studying the gaseous and solid atoms or molecules. The methods reveal unending fundamental phenomenon in atomic physics.

Machines like a small accelerator, a laboratory isotope separator or a conventional mass spectrometer are the sources for monoenergetic ions handled by the experimentalists.

In the present paper we shall describe a few experiments on atomic collisions which reveal the interference effects and channeling phenomena. The former is a quantum mechanical effect depicting the wave nature of atoms and molecules and the latter is based on a classical concept with an extensive application in solid state physics. Both the phenomena help us to obtain new findings in the fundamental behaviour of atomic collisions in gases and solids.

2. INTERFERENCE EFFECTS

(i) *Rainbow scattering*

In elastic collisions between atoms or molecules, rainbow scattering is a phenomenon compared to the optical rainbows. In figure 1, the geometry of

light rays in a raindrop forming rainbows are shown. With the increase of the miss distance r, the angle of the emergent light rays decrease to a minimum θ_r and then increases as r is further increased. The formation of a primary rainbow is explained without even the wave concept of light as done by Descartes with the geometry shown in figure 1. Light rays undergoing two or more internal reflections produce secondary or higher order ranbows in the same way. However, for details of the primary or secondary rainbows, a wave description is necessary, since rainbow angle is dependent upon the refractive index of water for light and the outer edges are less intense than what Descartes theory predicts. In optical

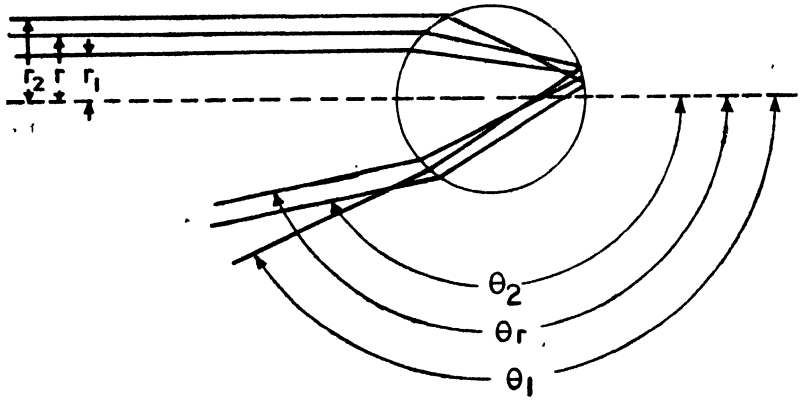

Fig. 1. Trajectories of light rays in a raindrop producing a rainbow.

rainbows, the interference effects produce supernumery rainbows inside the primary or secondary rainbow. The situation arises when two light rays emerging at the same angle enter two different points corresponding r_1 and r_2 in figure 1, they traverse slightly different amounts of water resulting in a phase difference. Depending on whether they are out of step by half a wave length or a full wave length, there will be fringes in the light intensity. The spacing between the two maxima of such rainbows depends on the wavelength of light and the diameter of the water drop. The spacing is greater for a smaller drop with a distinct maxima of a supernumery rainbow different from the primary one.

In figure 2, trajectories in the atomic scattering shown can be compared with fig. 1. The repulsive core is the dark circle surrounded by a sphere of attraction. Between these two spheres θ_r is the minimum deflection angle called rainbow angle. The scattered particles appear in more quantities near θ_r than nearby angles. So the intensity as a function of θ shows a maxima at θ_r producing the rainbow structure similar to optical phenomena. θ_r gives a direct measure of ϵ, the well depth of the interaction potential shown in figure 3.

In view of the classical theory, there will be a sharp spike of intensity at θ_r superposed on a background of small angle attractive scatterings by the outer

edge of the interatomic potential. The large angle scatterings due to repulsive core are weak and in an experiment both the repulsive and attractive scatterings in negative and positive angles can not be distinguished. Thus both types of the scattered particles will be superposed.

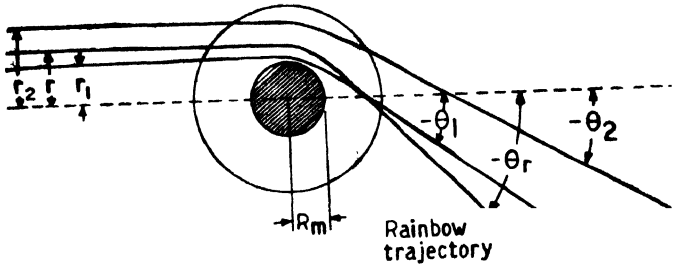

Fig. 2. Trajectories of atoms in a rainbow scattering in atomic collisions. The hatched circle is the repulsive core surrouded by a sphere of attraction in the target atom producing a minimum deflection at an angle θ_r, the rainbow angle.

But the wave nature of the atoms predicts the interference effect between the particles scattered due to the attractive and repulsive potentials resulting in

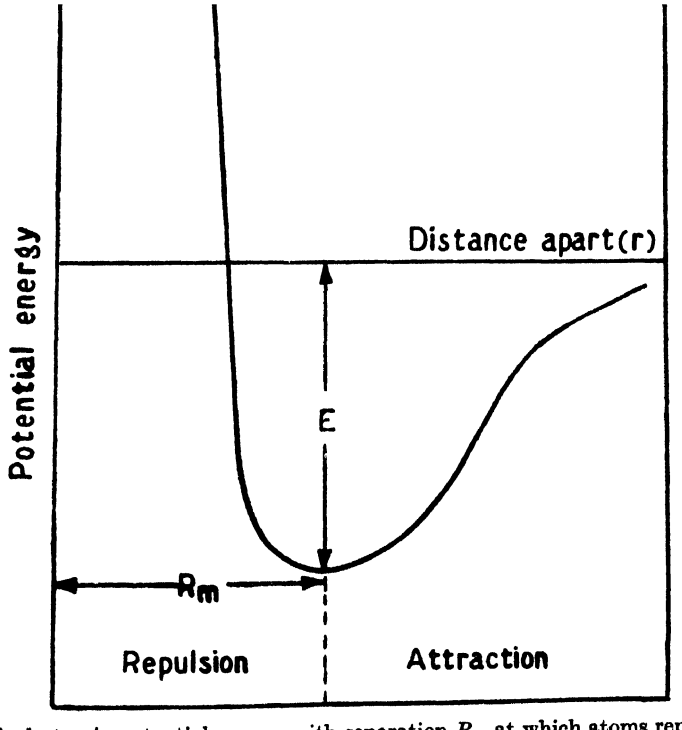

Fig. 3. Typical atomic potential anergy with separation R_m at which atoms repel each other and the depth of potential well ϵ.

a supernumery rainbow in the primary one, as in the optical phenomena. The maxima between such two supernumery rainbows depend on the length of the scattering potential R (figure 3) similar to the dependence of such maxima on the size of the raindrop in case of optical phenomana.

Many experiments have been carried out for collisions of alkali metal atoms with noble gases, Hg-alkali atoms or from molecules such as HBr and CCl_4 and the interference effects have been observed. We show here some experiments as an example in confirmation of the theoretical effects we have described. Figure 4 shows the rainbow effect with 1.(primary) 2.(secondary) 3. (tertiary) maxima

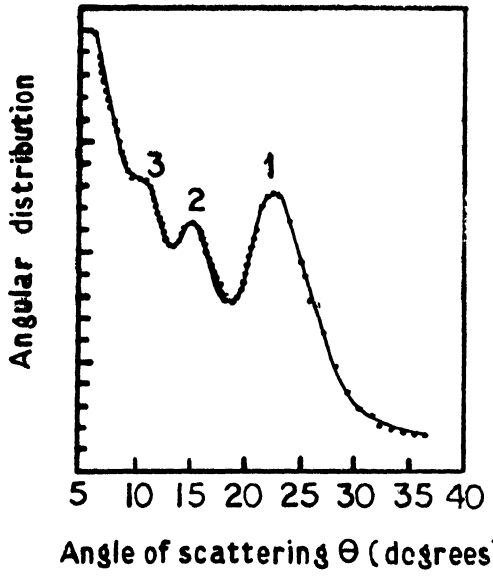

Fig. 4. Angular distribution for scattering of Na by Hg with low resolution showing 1. Primary, 2. Secondary and 3. Tertiary rainbow maxima. (Hundhausen and Pauly 1964)

observed by Hundhausen and Pauly (1964) using a crossed beam technique for scattering of Na by Hg. Figure 5 shows the results with an apparatus with increased resolution for scattering of Na by Xe observed by Barwig *et al* (1966). The curves show distinct finite structures of supernumery rainbows both in the primary and secondary ones.

(ii) *Nuclear symmetry effect*

Aberth *et al* (1965) report the observation of an interference effect appearing only in collisions involving identical nuclei with rainbow scattering. Here it is impossible to distinguish experimentally between a glancing collision that scatters the incident ions through an angle θ and a knock on collision with resonant

charge exchange that scatters the target as an ion to the detector at the same angle θ.

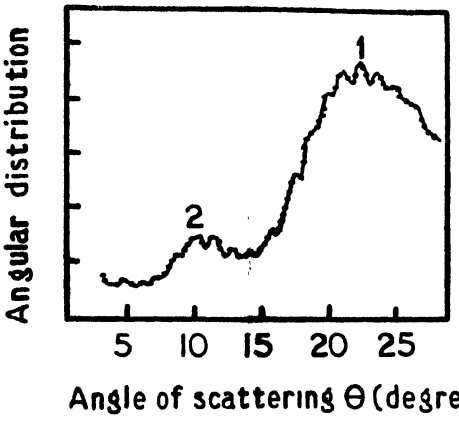

Fig. 5. Angular distribution multiplied by $\theta^{4/3}$ for a clear exposition of the supernumery structure in the primary and secondary rainbows observed for scattering of Na by by Xe with increased resolution. (Barwig *et al* 1966).

Classically the two processes involve contributions from very different regions of impact parameter and the observed cross-sections should be the sum of the two. Quantally an interference between the two processes is expected leading to secondary oscillations in $^4He^+ + He$. Such secondary oscillations are absent in $^4He^+ + {}^3He$ (Figure 6).

(iii) *Glory effect*

An optical glory effect is observed when a strongly forward or backward scattering of light occurs. A forward glory effect causes interference with the other forward trajectories determining the size of the scatterer or the total cross-section. Classically it is expected that the total crossection should smoothly decrease with increasing energy, since more energetic particles passing closer to the target are not appreciably deflected.

But some of the particles colliding with target anyhow are scattered without any deflection. These are the forward and glory trajectories shown in figure 7. An interference pattern is produced by those trajectories with the grazing ones. The glory trajectory has a phase difference causing the interference effect.

In one of the experiments, Rothe *et al* (1962) used a velocity selector and hot wire detector with mass spectrograph to measure the total crossection of Li colliding in Xe as a function of relative velocity. Figure 8 shows the results of the experiment exhibiting glory effect superposed on the smoothly varying curve

of average crosssection $\bar{Q}$. In the same fiture, the dashed curve illustrates the glory effect predicted by theory based on a potential of the form

$$V(R) = \epsilon f\left(\frac{R}{R_m}\right) \qquad \ldots (1)$$

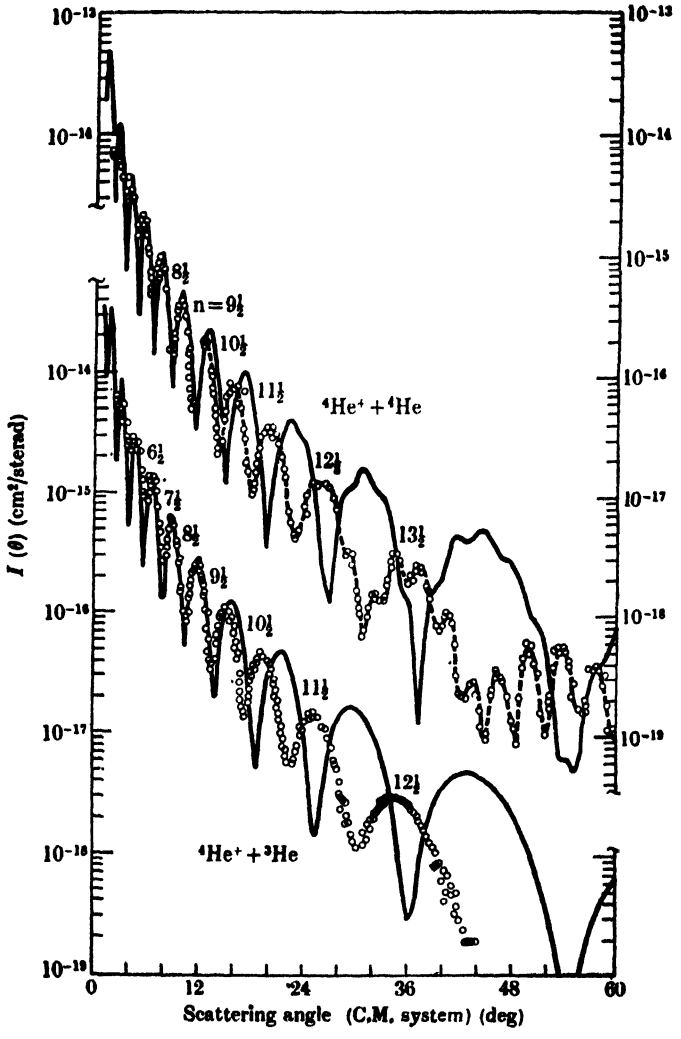

Fig. 6. Differential elastic crosssection $I(\theta)$ per unit solid angle for He^+-He collisions at 600 eV incident energy. Calculated by Marchi and Smith (1965) 000 observed by Aberth *et al* (1965).

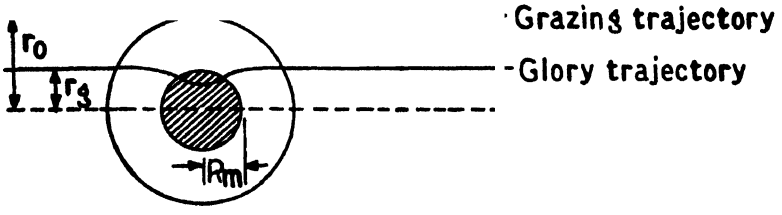

Fig. 7. Forward and Glory Trajectories for r_0 and r_g respectively and R_m is the separation at which atoms repeal each other.

where f is a suitable function and putting $n = 12$ in one of its forms suggested by Lennard-Jones (1924)

$$f(x) = \frac{6}{n-6}\frac{1}{x^n} - \frac{n}{n-6}\frac{1}{x^6} \qquad \ldots (2)$$

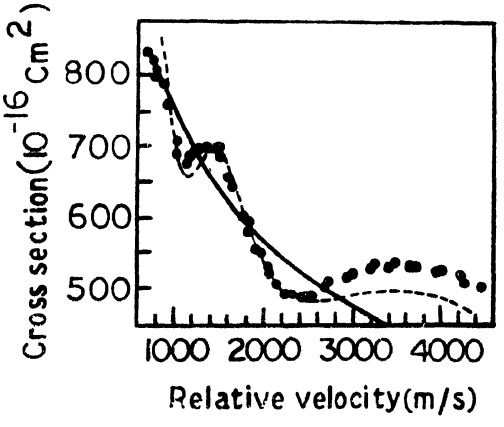

Fig. 8. Glory effect in Li-Xe collisions 000 experimental — theoretical (Rothe *et al* 1962).

and with

$$\epsilon = 2.01 \times 10^{-14} \text{ ergs and } R = 5.26 \times 10^{-8} \text{ cm}$$

In figure 8 the solid curve $\bar{Q}$ is calculated with the same interaction.

The scattering due to attractive potential is determined by

$$2\pi\epsilon R_m/hv > 1 \qquad \ldots (3)$$

where v is the relative velocity. Taking the repulsive core to be absent and the only Van der Waals attraction,—(C/r^6) is active we have

$$\bar{Q} = 8.08 \left(2\pi \frac{C}{hv}\right)^{2/5}. \qquad \ldots (4)$$

Due to the presence of the repulsive core the total cross section $\bar{Q}$ is the sum of

$$\bar{Q}+\Delta Q \qquad \ldots (5)$$

where

$$\bar{Q} \propto v^{-2/5} \qquad \ldots (6)$$

and ΔQ is an oscillatory structure as a function of v, Von Busch *et al* (1967) carried on an experiment to determine the variation of $\Delta Q/Q$ defined in (5) for collision of Na with Xenon. Figure 9 shows the oscillating structure due to the interference effect in glory phenomena observed in the same atomic collisions.

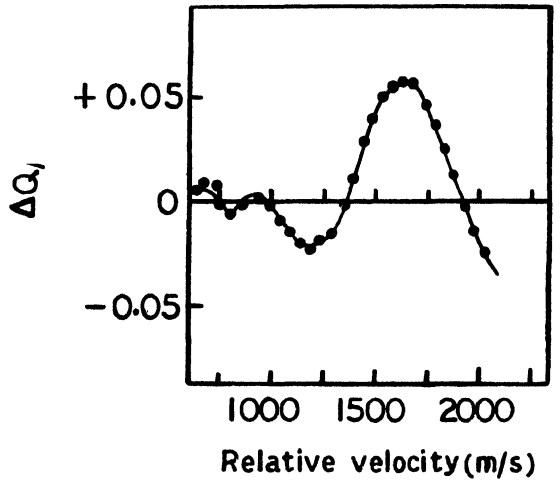

Fig. 9. $\Delta Q/Q$ versus v for Na and Xenon collisions showing glory oscillation (Von Bush *et al* 1967).

(iv) *Resonant charge transfer process*

A new line of experiments was initiated by Everhart and his group with an experiment on the angular distribution of scattered ions. In one of these experiments they for the first time observed interference fringes in symmetric ion atom charge transfer scattering as a function of energy at fixed angle and later as a function of angle at fixed energy. The oscillating pattern represents an interference between even (g) and odd (u) electronic states of molecular ion system. Fig 10 shows the apparatus used by Ziemba and Everhart (1959) for studies of the angular distribution of the scattered primary ions in the fast atomic collisions. Figure 11 shows a comparison of the observed value of P_{tr}, probability of charge transfer of H^+ in H and the values calculated by the pseudostate expansion method.

The observed values of P_{tr} is notable in the sense that it instead of oscillating between 0 and 1 oscillates with damping due to interference between gerade and ungerade states of H_2^+ ion.

A large number of experiments with various projectiles and targets confirm the interference effect in resonant charge transfer process.

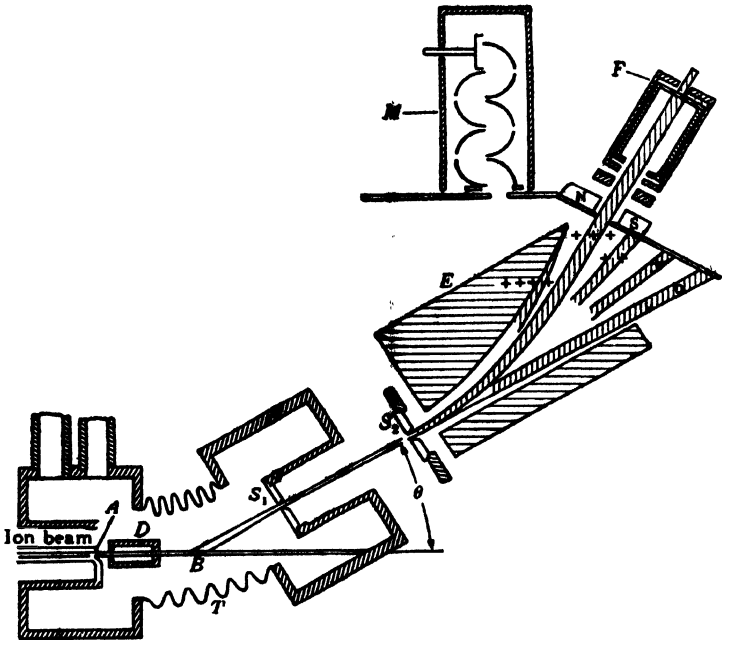

Fig. 10. Apparatus used by Ziemba and Everhart (1959) for measuring angular distribution in Resonant charge transfer process. Scattering chamber T, defining apperture A, collimating apertures S_1, S_2, electrostatic analyser E. Faraday cage for detecting primary beam, D, Multiplier, M and Faraday case, F for recording the charge states from 0 to 7. Particles scattered at B.

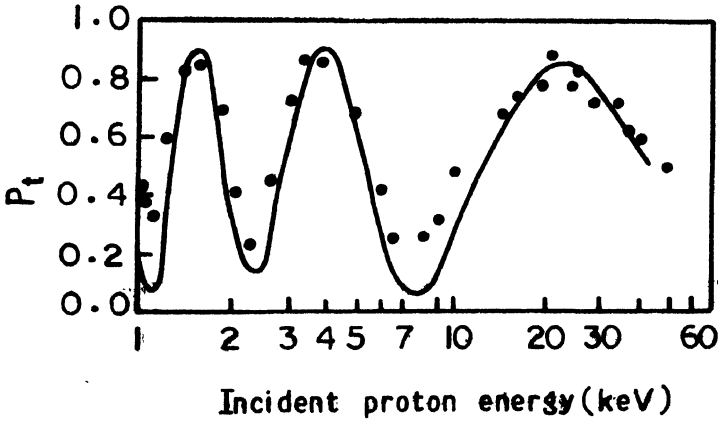

Fig. 11. P_{tr} vs incident proton energy for H^+-H charge transfer at a scattering angle 3° in the laboratory system ...expt;—theory. (Helbig and Everhart 1965).

Erickson and Smith (1975) observed a similar interference effect in the charge transfer collisions between low energy He^+, Ne^+, Ar^+ as projectiles and Pb or Ge crystal as targets by ion scattering spectrometry (ISS). Fig. 12 shows $^4He^+$ ion yield versus ion energy for $^4He^+$ colliding with Pb and Germanium. In the charge transfer model He^+ and the surface atom form a quasi-molecular stae, when the incident ion captures an electron of the surface atom and is neutralised. Such neutralisation results in a decrease in He^+ ion yield detected by ISS. The oscillatory structure in Fig 12 is due to interference between the electronic states of molecular ion.

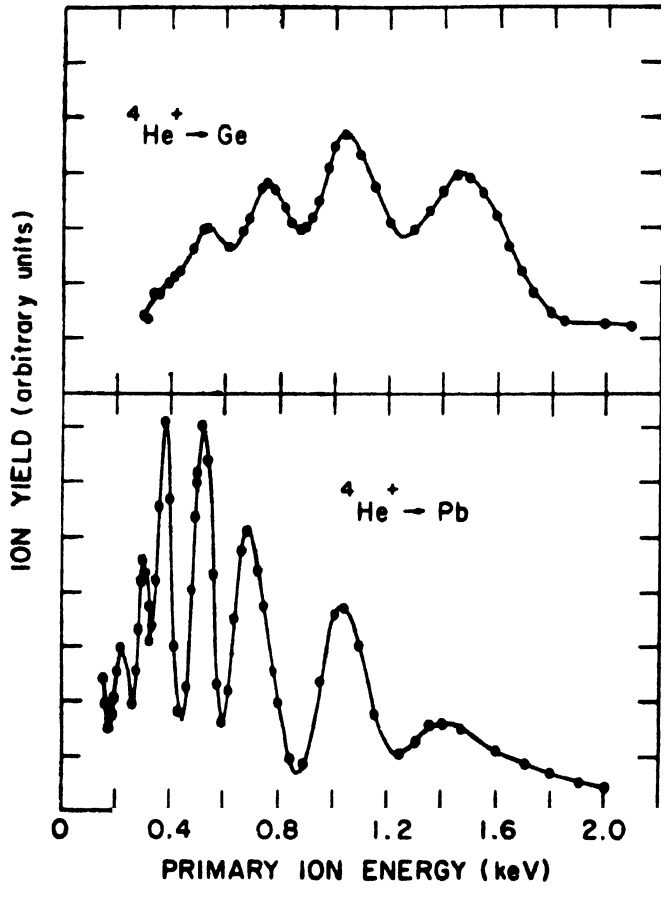

Fig. 12. Charge transfer of $^4He^+$ with Pb and Ge detected by ISS (Erickson and Smith 1975).

The above charge transfer being asymmetric i.e. A+B A+B$^+$+and for this quasi-resonant chargo transfer the initial-state and final-state electronic energies be nearly degenerate. For *d*-electron energy levels of Pb and Ge being ~10 ev and I.P. of He being 24.6 ev, the above condition is satisfied. For elements with greater energy separation no oscillatory structure is observed. Tolk *et al* (1976)

measured the relative intensity of $^4He^+$ as a function $1/v$ for several scattering angles θ for Pb and GaP target in the energy range 200-3000 eV of He^+. The results show that the intensity of scattered He^+ oscillates as a function of incident energy in agreement with the observations of Erickson and Smith (1975). A semi-quantitative model of the process worked out by Tolk *et al* (1976) predicts the phase difference between the two electronic states of the molecular ion to be

$$\Delta\varphi = (2/\hbar v) <ER> \quad \ldots (7)$$

From the experimental results the value of $<ER>$ is extracted to be 17.7 and 23.5 ev Å for He on Pb and GaP respectively. The numbers may be compared to the estimates 22 and 19 ev Å found by calculations based on the approximate exchange splitting with Slater type functions of the appropriate symmetry and binding energy (Tolk *et al* (1976) Ref. 6).

(v) *Total charge transfer and excitation cross sections*

Similar to the glory oscillations in the elastic atomic collissions, an interesting feature of oscillatory structure reveals in the measurements of alkali ion atom total charge transfer crosssections as a function of incident ion energy observed by Perel *et al* (1965a, b), Marino (1966), Perel and Yahiku (1967), Daley and Perel (1969), Perel *et al* (1969). The oscillations are superposed on a smoothly varying curve and are regularly spaced with $1/v$ of the ions and their amplitude increases with ion energy for both the symmetric and asymmetric charge transfer collisions. Smith (1966) showed that for symmetric charge transfer collisions such oscillat,ons can be explained, when the potential dfference between gerade and ungerade states of the quasimolecule passes through a maximum. In figure 13, the results

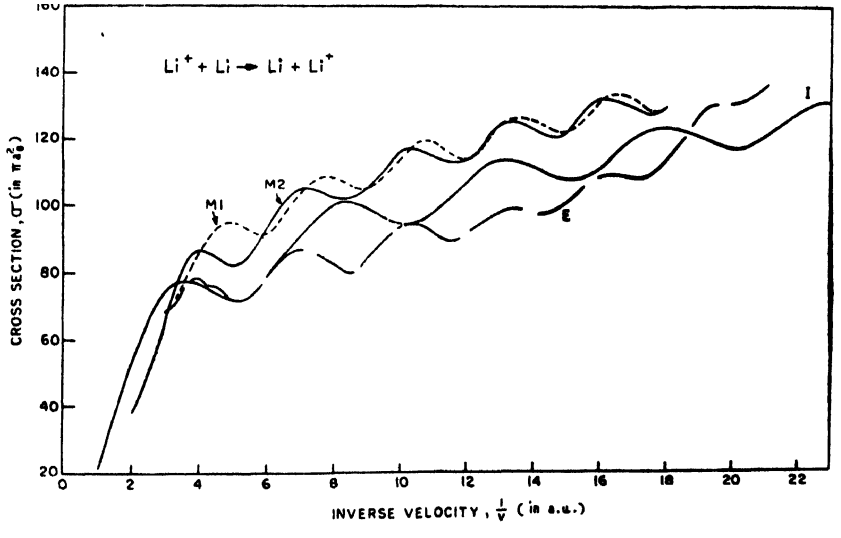

Fig. 13. Total charge transfer crosssection σ as a function of $1/v$ for Li^+-Li collision. M_1, M_2 and I are theoretical curves (see text).

of one of the experiments with a crossed beam technique by Daley and Perel (1969) are given showing oscillations of total charge transfer crosssections for Li^+—Li as a function of inverse velocity. In the same figure M_1 and M_2 are the curves given for comparison obtained by McMilan (1971) and calculated on the basis of an expansion in two state and three state approximation respectively of the molecular eigenfunction whereas I is the curve obtained by Dewangan (1974) based on the expansion of the atomic eigen functions in the two state theory. Fig. 14 (Dewangan 1974) shows the anomaly in the charge transfer probability

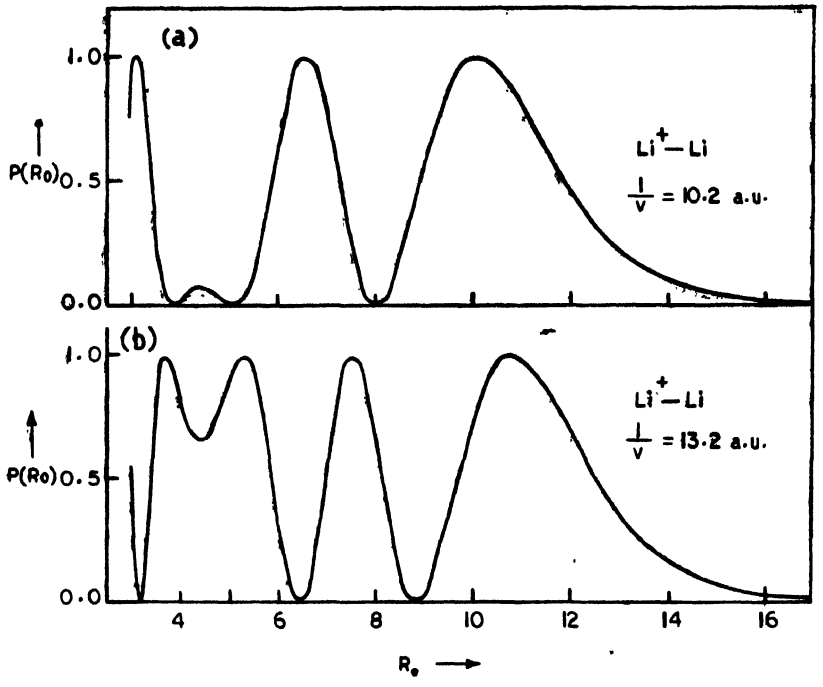

Fig. 14. Total charge transfer probability $P(R_0)$ as a function of the impact parameter R_0 for Li^+-Li collision for two values of v^{-1}, (a) 10.2 a.u. (b) 13.2 a.u.

$P(R_0)$ for Li^+--Li as a function of impact parameter, (a) for $1/v = 10.2$ a.u. and (b) for $1/v = 13.2$ a.u. In (a) two oscillations are merged to give a broad anomalous oscillation near the stationary point $R_0 = 4.4$ of $X(R_0)$ which contributes to an oscillation maximum in the total crosssection. The anomalous oscillation in (b) around $R_0 = 4.4$ contributes to an oscillation minimum in the total cross-sections. Here

$$P(R_0) = \sin^2 \left(\frac{X(R_0)}{v} \right. \qquad \ldots (8)$$

in which $$X(R_0) = \int^{\infty} XI(R)dR \qquad (9)$$

with $$XI(R) = \frac{H'_{fi} - H'_{ii}\, S}{1 - S^2} \quad \ldots (10)$$

where

$$H'_{fi} = \int \psi_f^*\, H' \psi_i d\tau \quad \ldots (11)$$

$$H'_{ii} = \int \psi_i^*\, H' \psi_i db \quad \ldots (12)$$

$$S = \int \psi_f^* \psi_i d\tau = \int \psi_i^*\, \psi_f\, d\tau \quad \ldots (13)$$

Where H' is the interaction Hamiltonian, ψ_i and ψ_f are wave functions of the initial and final states respectively. Dewangan *et al* (1972a, 1972b) have calculated $Li^+ - Li$ and $Na^+ - Na$ charge transfer crosssection well agreeing to the experimental results by Perel *et al* (1969) and Daley and Perel (1967) respectively. Lichten (1965) points out the similarity between the oscillations in the total charge transfer crosssections and those observed in the resonant electron capture probability (Ziemba *et al* 1960) due to an interference effect as discussed in sec 4.

Zavilopulo *et al* (1973) investigated the total excitation and charge transfer crosssections for $Mg^+ - Rb$ and Mg^+-Cs collisions in the energy range 4-1000 eV.

The two inelastic channels are

$$Mg^+ + Rb \nearrow Mg^+ + Rb^*(^2P_{3/2}) + 1.59\ eV \quad \ldots (14)$$
$$\searrow Mg^*(4^3S_1) + Rb^+ + 1.64\ eV \quad \ldots (15)$$

and in $Mg^+ - Cs$

$$Mg^+ + Cs \nearrow Mg^+ + Cs^*(6^2P_{3/2}) + 1.46\ eV \quad \ldots (16)$$
$$\searrow Mg^*(4^3S_1) + Cs^+ + 1.36\ eV \quad \ldots (17)$$

Fig 15(i) shows the extrema for both transitions of the Rb atom ($\lambda = 7800$Å) and Mg atom ($\lambda = 5184$Å) are equidistant with a period $\Delta\nu^{-1} = 8.5 \times 10^{-8}$ sec/cm and they are in counterphase satisfying the law of conservation of the total probability of population of the levels of the quasi-molecule Mg^+Rb. Similar effect is produced in case of $Mg^+ - Cs$ shown in Fig. 15(ii) along with a new feature of two regular periods of the oscillations of the total level excitation crosssections.

Anderson *et al* (1974) performed experiments to measure excitation and charge transfer crosssection for ions ranging from Li^+ to Al^+ as projectiles with energies varying from 0.1 to 15 KeV using Ne as the target. Interference between direct excitation and charge transfer collision channels leading to regular oscillations, 180° out of phase have been observed in $N^+ - Ne$, $O^+ - Ne$, $Na^+ - Ne$ and $Mg^+ - Ne$ systems.

3. Channeling Phenomena

When a fast ion beam collides with a single crystal, the repulsive potential of the atoms of the crystal directs the ions of suitable energy and direction of

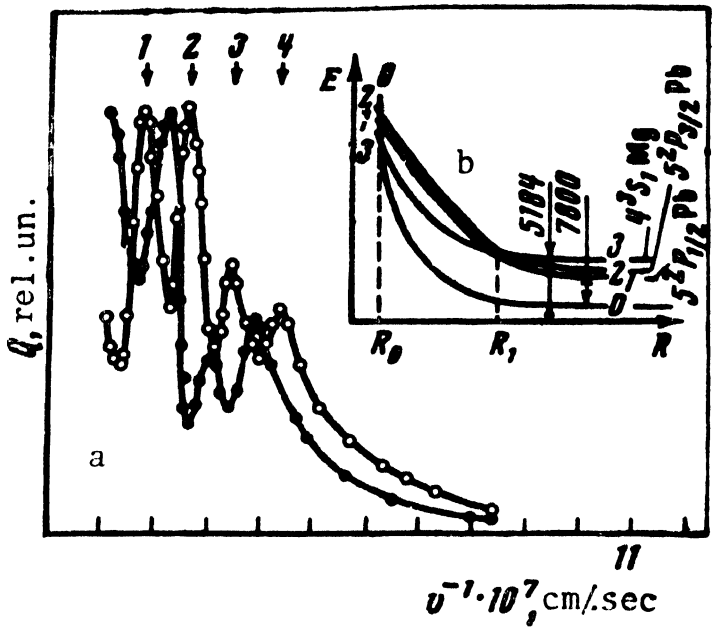

Fig. 15. (i)[a) relative crosssections Q for the excitation of the $\lambda = 5184$Å Mg line (light circles) and $\lambda = 7800$Å Rb line (dark circles) plotted against $1/v$. b) Term scheme of the quasimolecule Mg+Rb (ii) a) Relative cross sections for the excitation of the Cs line $\lambda = 8512$Å (dark circles) and $\lambda = 5184$Å Mg line (light circles) against $1/v$. b) Term scheme of the quasimolecule (Mg^+Cs).

incidence through the open channel of the crystal acting like an open tube suffering minimal energy loss due to successive small angle scattering. The phenomena is classically explained by the theory of Lindhard *et al* (1963). A sort of simple focussing of ions exists in the more open channels of a crystal and an assisted focussing in the less open ones. Here, we present a few experimental results on the influence of channeling on the sputtering of single crystals by ions and back scattering of ions by single crystals. For further references and critical discussions on the details reference may be made to Gemmel (1974), Morgan (1973) and Dearneley (1973).

(i) *Sputtering*

When atoms of a single crystal are sputtered by fast ions, a part of the ion beam is channeled through the crystal and another part is random or nonaligned beam responsible for sputtering. Using the ion beam of Ar^+, Kr^+ and Xe^+ from an electromagnetic isotope separator, a monocrystalline silver was sputtered and the yield was compared with the yield calculated on the model given by Onderdelinden (1966) based on the channeling theory of Lindhard (1965).

Fig 16 shows the comparison of the measured sputtering yield (Bhattacharya and Karmohapatro 1974) for normally incident Ar^+ ions on (111) and (100) Ag crystals as a function of ion energy with the calculated yield from the theory for three values of X_0, the thickness of the layer important for sputtering. Influence of channeling on the sputtering phenomena is prominent in the work by Dey *et al* (1970), Basu *et al* (1971) and Onderdelinden (1968).

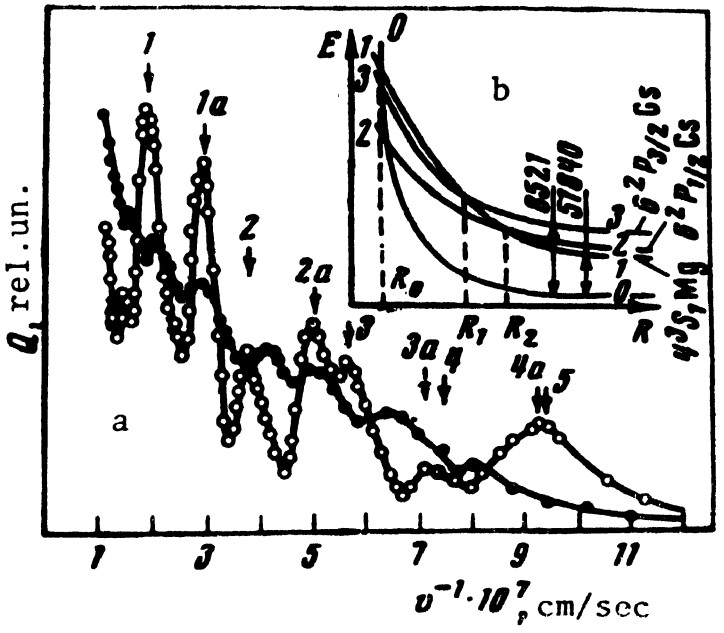

Fig. 15(ii). Sputtering yield S of Ag crystals as a function of energy of the colliding ions Ar^+. Experimental points are compared with theory for three values of X_0 – – – 60Å; –.–. 90Å; —75Å.

In a second experiment by Bhattacharya (1974) the sputtered atoms were collected from single crystals on a quartz plate. Visible deposits showing orientation dependent patterns were found to form on the plate after an irradiation of about 15 minutes with 20μA beam. Fig 17a shows the experimental setup and the orientation dependence of the deposition. Fig 17b shows the spots of the pattern due to <100> and <110> axis of a Ag (111) crystal normal to the ion beam (Bhattacharya *et al* 1975). A microdensitometer plot of the deposit pattern of Fig. 17b gives the relative intensities and widths of the <110> and <100> spots shown in Fig 18. The wider peak C in Fig 18 confirms the classical model of an assisted lens focussing by four atoms forming a ring which is weaker than the simple focussing in <110> axis of a Ag (111) crystal.

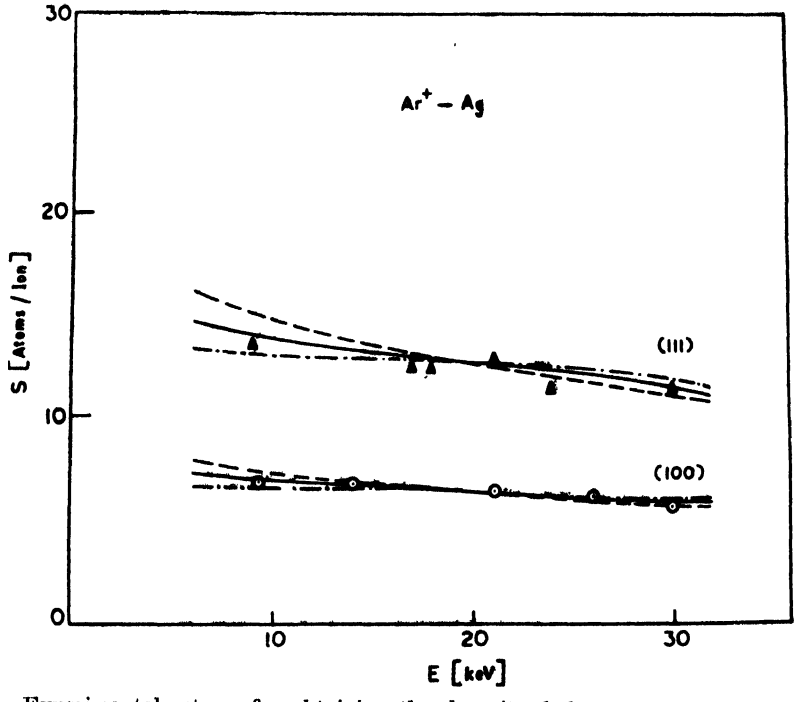

Fig. 16. Experimental set up for obtaining the deposit of the sputtered atoms and the orientation dependence of the deposit pattern.

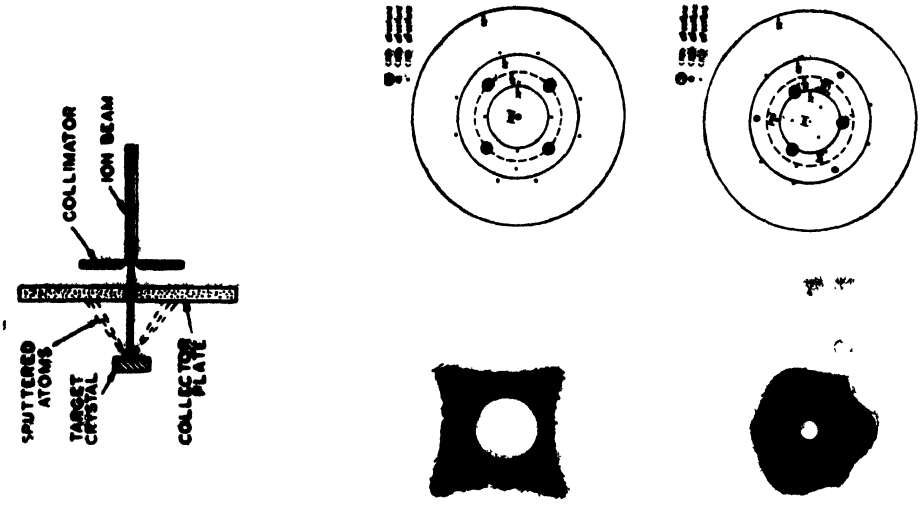

Fig. 17a. Experimental set up for obtaining the deposit of the sputtered atoms and the orientation dependence of the deposit pattern.

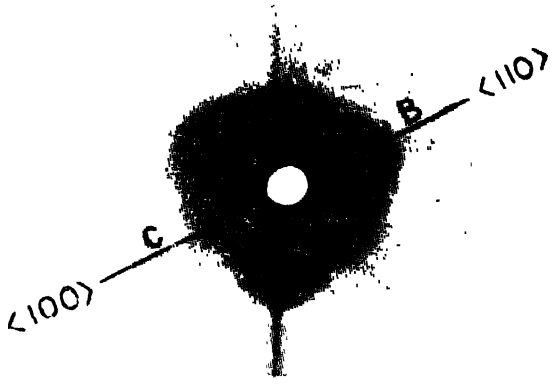

Fig. 17b. <100> and <110> spots in the deposit from a Ag (111)crystal bombarded by Ar^+ ions.

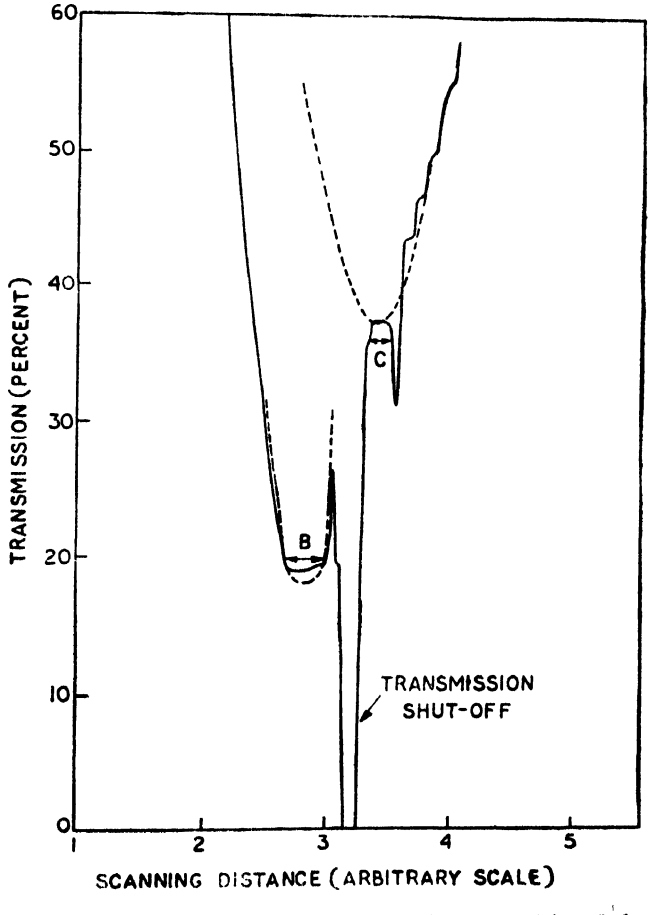

Fig. 18. Reproduction of a microdensitometer response for the widths of the <110> and <100> spots at B and C in Fig. 17b.

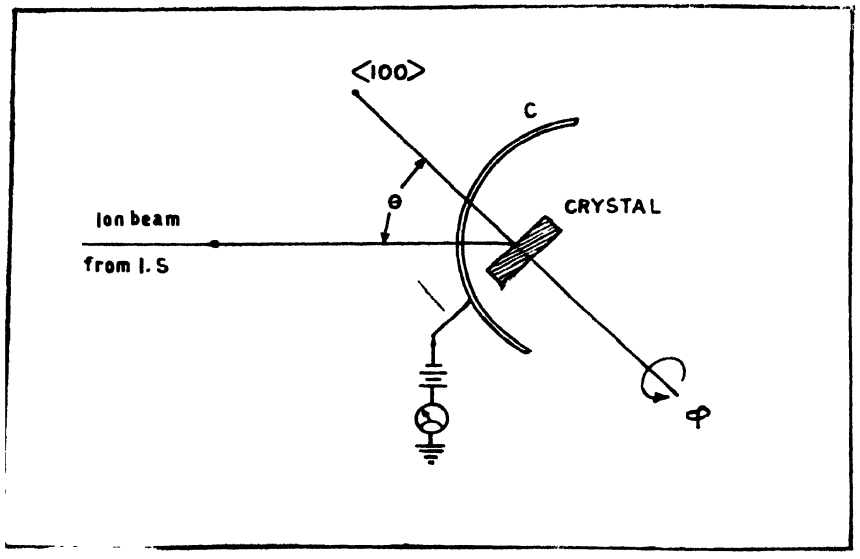

ig. 19. Experimental set up for back scattering experiment on Ag (100) crystal.

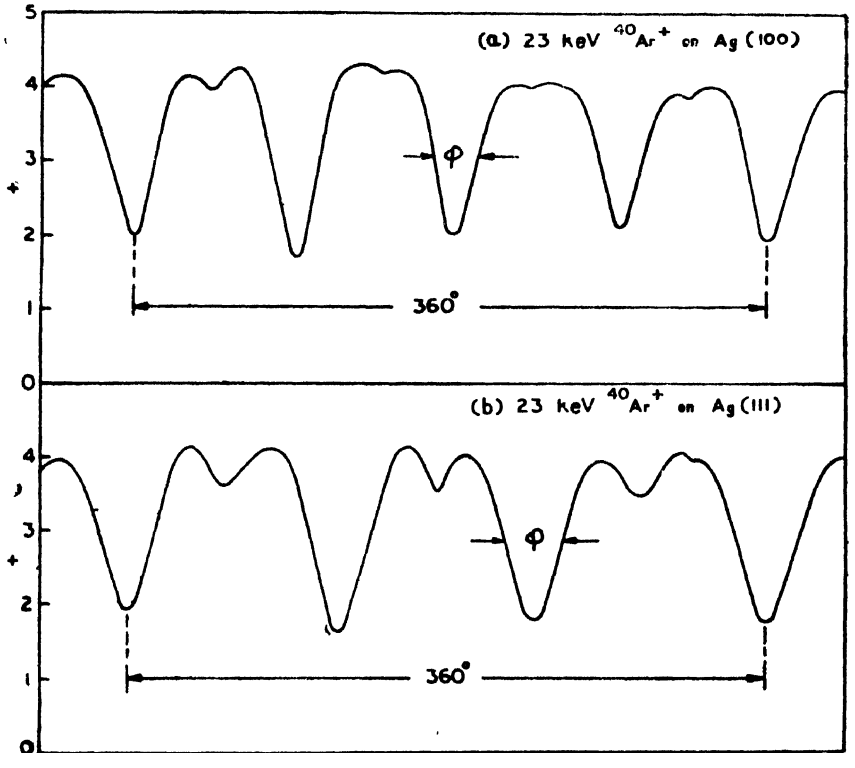

Fig. 20. (a) Yield of back scattered ions from Ag (100) with four minima (b) Yield of back scattered ions from Ag (111) crystal with three minima.

(ii) *Back scattering*

Whenever an energetic ion beam enters a low index direction of a single crystal the back scattered current shows minima due to channeling. We reproduce here an experiment showing the influence of channeling on the back scattering of ions done by Bhattacharyya and Karmohapatro (1973). Fast ions from an EMIS collides on a silver (100) crystal at an angle 45° with its plane. Fig 19 shows the experimental arrangement of the set up of the crystal showing rotation given in course of experiment with fixed $\theta = 45°$. Fig 20a shows the yield of the back scattered ions with four pronounced minima for the alignment of othe ion beam with the <110> direction for four values of ϕ in one full rotation, because of the four fold symmetry of an f.c.c. crystal with respect to its <100> axis.

Fig. 20(b) shows three pronounced minima for the back scattered ion beam aligned with the <110> direction for three values in one rotation, because of the three fold symmetry of an f.c.c. crystal with respect to its <111> axis, when in a second experiment one Ag (111) crystal is placed as a target with $\theta = 35.3°$ with incident ion beam and the yield of the back scattered ions is measured.

4. Conclusions

It may be mentioned that the atomic collision phenomena reveals many fundamental aspects of physics not even guessed earlier. Recent experiments tend to focuss our attention to a broader field of physics of gases and solids covering the disciplines like plasma physics and solid state physics. When nuclear physics or high energy physics experiments unveil many unknown facts, atomic collision experiments give us details of the known area of physics and add a new dimension for the future experiments.

References

Aberth W., Lorents D. C., Marchi R. P. and Smith F. T. 1965 *Phys. Rev. Lett.* **14**, 776.

Anderson T., Kirkegaard-Nielasen A. and Olsen K. J. 1974 *Phys.* **A10**, 2174.

Barwing P., Buck U., Hundhausen E. and Pauly H. 1963 *Phys Rev.* **130**, 2333.

Basu D., Dey S. D. and Karmohapatro S. B. 1971 *Nucl Inst. and Methods* **93**, 403.

Bhattacharyya R. S. 1974 *Ph.D. Thesis*, Calcutta University.

Bhattacharya R. S., Basu D. and Karmohapatro S. B. 1974 *Radiation effects* **21**, 215.

Bhattacharya R. S. and Karmohapatro S. B. 1973 *Nucl. Inst. and Methods* **109**, 191.

Daley H. L. and Perel J. 1969 *Proc. of Sixth Int. Conf. on Physics of Electronic and Atomic Collision* p.1051 (The M.I.T. Press).

Dearnaley G. 1973 *Ion Implantation* (S. Amelinckx, R. Gevers and J. Nihoul, eds.) p. 9, N.H. Pub., Amsterdam.

de Heer F. J. 1956 Ph.D. Thesis, Amsterdam.

Dewangan D. P. 1974 *Ind. Jour. Phys.* **48**, 269.

Dewangan D. P., Mukherjee D. K. and Karmohapatro S. B. 1972a *Phys. Rev.* **A5**, 1755.

Dewangan D. P. Mukherjee D. K. and Karmohapatro S. B. 1972b *Phys. Rev. Letters* **28**, 583.

Dey S. D., Basu D. and Karmohapatro S. B. 1968 *Nucl. Inst and Methods* **61**, 260.

Erickson R. L. and Smith D. P. 1975 *Phys Rev. Letters* **34**, 297.

Gommol D. S. 1974 *Rev. Mod. Phys.* **46**, 129.
Helbig H. F. and Everhart E. 1965 *Phys. Rev.* **A140**, 715.
Hundhausen E. and Pauly H. 1964 *Z. Naturf.* **19A**, 810.
Karmohapatro S. B. 1976 *Adv. Electronics and Electrophysics* 42, p. 113 (Academic Press).
Lennard-Jones J. E. 1924 *Proc. Roy. Soc.* **A106**, 441.
Lichten W. 1965 *Phys. Rev.* 139, **A27**.
Lindhard J. 1965 *Kgl. Danske. Vid. Selsk, Matt. Fys. Medd.* 34 No. 14.
Lindhard J., Scharff M. and Schigtt H. E. 1963 *Kgl. DanskeVid. Selsk. Matt. Fys. Medd.* **33**, Nl. 14.
Marchi R. P. and Smith F. T. 1965 *Phys. Rev.* **A139**, 1025.
Marino L. 1966 *Phys. Rev.* **152**, 46.
Massey H. S. W. and Gilbody H. B. 1974 *Electronic and Ionic Impact Phenomena* second Edition, Vol. III and IV, Oxford University Press.
McMilan W. L. 1971 *Phys. Rev* **A4** 69.
Morgan D. V. ed 1973 *Channeling -Theory, Observation and Applications* Wiley, New York.
Onderdelinden D. 1966 *App. Phys. Letters* **8**, 189.
Onderdelinden D. 1968 *Thesis*, Univ. of Leiden p. 63.
Perel J., Daley H. L., Peek J. M. and Green T. A. 1969 *Phys. Rev. Letters* **23**, 677.
Perel J., Vernon R. H. and Daley H. L. 1965a *Phys. Rev.* **138A**, 937.
Perel J., Vernon R. H. and Daley H. L. 1965b *Proc. of Fourth Int. Conf. on Physics of Electronic and Atomic Collisions*, Quebec (Science Book Crafters, Hastingson-Hudson 1965) p.336.
Perel J. and Yahiku A. Y. 1967 *Proc. of Fifth Int. Conf. on Physics of Electronic and Atomic Collisions*, U.S.S.R. (Nauka Publ. House, Leningrad, U.S.S.R. 1967) p. 400.
Rothe E. W., Rol, P. K., Trujillo S. M. and Neynaber R. H. 1962 *Phys. Rev.* **128**, 659.
Sluyters T. J. M. 1959 *Physica* **25**, 1376 and 1389.
Smith F. J. 1966 *Phys. Lett* **20**, 271.
Tolk N. H., Tully J. C., Kraus J., White C. W. and Neff S. H. 1976 *Phys. Rev. Letters* **36**, 747.
Van Eck J. and Kistemaker J. 1962 *Proc. of 5th Int. Conf. Ionisation Phenomena in gases*, p. 51.
Van Eck J., de Heer F. J. and Kistemaker J. 1962. *Physica* **26**, 629.
Von Busch F., Strunck H. J. and Schlier Ch. 1967 *Z. Phys.* **199**, 518.
Zavilopulo A. N., Zapesochnyi I. P., Panev G. S., Skalko O. A. and Shepnik O. B. 1973 *JETP Letters* **18**, 245.
Ziemba F. P. and Everhart E. 1959 *Phys. Rev. Lett.* **2**, 299.
Ziemba F. P., Lockwood G. J., Morgan G. H. and Everhart E. 1960 *Phys. Rev* **118**, 1552.